Eur. J. Mineral., 35, 665–678, 2023
https://doi.org/10.5194/ejm-35-665-2023
© Author(s) 2023. This work is distributed under
the Creative Commons Attribution 4.0 License.

European Journal of Mineralogy
Open Access

First measurements of the Fe oxidation state of spinel inclusions in olivine single crystals from Vulture (Italy) with the in situ synchrotron micro-Mössbauer technique

Giulia Marras[1], Gabriele Carnevale[2], Antonio Caracausi[3,4], Silvio Giuseppe Rotolo[2,3], and Vincenzo Stagno[1,5]

[1]Dipartimento di Scienze della Terra, Sapienza Università di Roma, Rome, Italy
[2]Dipartimento di Scienze della Terra e del Mare, Università degli Studi di Palermo, Palermo, Italy
[3]Istituto Nazionale di Geofisica e Vulcanologia, Sezione di Palermo, Palermo, Italy
[4]Departamento de Geología, Universidad de Salamanca, Salamanca, Spain
[5]Istituto Nazionale di Geofisica e Vulcanologia, Sezione di Roma, Rome, Italy

Correspondence: Giulia Marras (giulia.marras@uniroma1.it) and
Vincenzo Stagno (vincenzo.stagno@uniroma1.it)

Received: 13 February 2023 – Revised: 6 June 2023 – Accepted: 30 June 2023 – Published: 21 August 2023

Abstract. The redox state of the Earth's upper mantle (i.e., oxygen fugacity, f_{O_2}) is a key variable that influences numerous processes occurring at depth like the mobility of volatile species, partial melting, and metasomatism. It is linked to the oxidation state of peridotite rocks, which is normally determined through the available oxythermobarometers after measuring the chemical composition of equilibrated rock-forming minerals and the Fe^{3+} in redox-sensitive minerals like spinel or garnet. To date, accurate measurements of Fe^{3+} / $\sum$Fe in peridotites have been limited to those peridotites (e.g., harzburgites and lherzolites) for which an oxythermobarometer exists and where spinel (or garnet) crystals can be easily separated and measured by conventional ^{57}Fe Mössbauer spectroscopy. Wehrlitic rocks have been generally formed by the interaction of a lherzolite with carbonatitic melts and, therefore, have recorded the passage of (metasomatic) fluids at mantle conditions. However, no oxythermobarometer exists to determine their equilibrium f_{O_2}.

The aim of this study was to retrieve the f_{O_2} of the mantle beneath Mt. Vulture volcano (Italy) through the study of a wehrlitic lapillus emitted during the last eruption ($\sim$ 140 kyr ago) that contain olivines with multiple tiny spinel inclusions with sizes < 40 µm. To our knowledge, the Fe oxidation state of these inclusions has been never determined with the Mössbauer technique due to their small sizes.

Here, we present measurements of the Fe^{3+} / $\sum$Fe using in situ synchrotron Mössbauer spectroscopy coupled with chemical and spectroscopic analysis of both host olivine and spinel inclusions.

The results show Fe^{3+} / $\sum$Fe ratios of 0.03–0.05 for olivine and 0.40–0.45 for the included spinels, the latter of which appear higher than those reported in literature for mantle spinel harzburgites and lherzolites. Given the evidence of the mantle origin of the trapped spinels, we propose that the high f_{O_2} (between 0.81 and 1.00 log above the fayalite–magnetite–quartz buffer; FMQ) likely results from the interaction between the pristine spinel lherzolite and a CO_2-rich metasomatic agent prior to the spinel entrapment in olivines at mantle depths.

Published by Copernicus Publications on behalf of the European mineralogical societies DMG, SEM, SIMP & SFMC.

1 Introduction

The redox state of Earth's interior plays a fundamental role in petrological processes including magma genesis, metasomatism, and deep volatile cycle. To date, the redox state of the Earth's upper mantle has been constrained by studying the chemical composition of rock-forming minerals in mantle xenoliths (i.e., peridotites and eclogites) supported by measurements of $Fe^{3+} / \sum Fe$ of redox-sensitive minerals like spinel and garnet. A linear correlation exists as reported by Stagno (2019) between the $Fe^{3+} / \sum Fe$ of equilibrated spinels or garnets and the oxygen fugacity (f_{O_2}) calculated using common oxythermobarometers (Ballhaus et al., 1991; Gudmundsson and Wood, 1995; Stagno et al., 2013), such as

$$\underset{\text{fayalite}}{6Fe_2^{(2+)}SiO_4} + O_2 = \underset{\text{ferrosilite}}{3Fe_2^{(2+)}Si_2O_6} + \underset{\text{magnetite}}{2Fe^{(2+)}Fe_2^{(3+)}O_4} \quad (1)$$

and

$$\begin{aligned} &\underset{\text{grossular}}{2Ca_3Al_2Si_3O_{12}} + \underset{\text{fayalite}}{4Fe_2^{(2+)}SiO_4} + \underset{\text{enstatite}}{6MgSiO_3} + O_2 \\ &= \underset{\text{andradite}}{2Ca_3Fe_2^{(3+)}Si_3O_{12}} + \underset{\text{pyrope}}{2Mg_3Al_2Si_3O_{12}} \\ &+ \underset{\text{ferrosilite}}{4Fe^{(2+)}SiO_3}. \end{aligned} \quad (2)$$

This allows, at first approximation, an independent qualitative estimate of the redox state of mantle rocks simply by looking at the Fe oxidation state in these minerals in the case of lack of other silicates as required by the application of equilibria in Eqs. (1) and (2). To date, accurate measurements of $Fe^{3+} / \sum Fe$ in minerals have been performed with conventional and milliprobe Mössbauer spectroscopy (McCammon, 2004; Frost and McCammon, 2008), a technique that generally bypasses technical issues such as matrix effects, crystal orientation, and the need for proper standards as in the case of alternative techniques like X-ray absorption near-edge structure (XANES) for glasses (Cottrell et al., 2009; Berry et al., 2003) and minerals (Wilke et al., 2001, 2005; Dyar et al., 2002, 2016; Schmid et al., 2003; Rudra et al., 2021); the Flank method with an electron microprobe (EPMA; Fialin et al., 2007; Hoefer et al., 2003; Höfer and Brey, 2007; Longo et al., 2011); stoichiometric calculations also performed with an electron microprobe (Droop, 1987; Wood and Virgo, 1989; Sobolev et al., 1999; Davis et al., 2017). However, due to the limited spatial resolution of the Mössbauer apparatus ($> 100\,\mu m$; McCammon, 1994), the oxidation state of micrometric inclusions (e.g., $< 50\,\mu m$) such as those trapped in minerals and, in turn, the role that these might have on mineral redox equilibria can be difficult to address. A great improvement of the spatial resolution of this technique is provided by the high-brilliance source for synchrotron Mössbauer spectroscopy (SMS) at beamline ID18 of the European Synchrotron Radiation Facility (ESRF, Grenoble) (Potapkin et al., 2012). Here, the spot area being as small as $\sim 3 \times 8\,\mu m^2$ allows challenging micrometer-scale investigation of the $Fe^{3+} / \sum Fe$ ratio in minerals to be performed. Such a technique has brought tremendous improvement to the quality of the measurement of Fe oxidation state in minerals trapped in lithospheric and sub-lithospheric diamonds (Nestola et al., 2016; Faccincani et al., 2022; Kiseeva et al., 2018, 2022) as well as that of minerals displaying either chemical zonation (e.g., garnet) or late-stage alteration (e.g., clinopyroxene) as discussed by Mikhailenko et al. (2020). In the former, the measurements of $Fe^{3+} / \sum Fe$ are possible due to the transparency of the diamond host to the X-rays, while in the latter case point measurements on the core and rim of a mineral are made possible by the combined collimated synchrotron radiation and the motorized stage with micrometric precision (Nestola et al., 2016) that allows spectra acquisition from the desired area. Therefore, this technique can be further applied to micrometer inclusions trapped in minerals other than diamonds that display a poikilitic texture.

Spinel occurs as a primary mineral both in intrusive and volcanic igneous rocks. Those occurring in mantle peridotites are of fundamental importance to constrain the depth of the host rock (Frost, 2008), as well as the extent of partial melting experienced by the source rock (e.g., Hellebrand et al., 2001). In addition, important oxythermobarometric calculations on mantle rocks and crystallized lavas are made possible by the coexistence of spinel with another rock-forming mineral like olivine (Eq. 1, Ballhaus et al., 1991; O'Neill et al., 1987; Wood and Virgo, 1989; Mallmann and O'Neill, 2013; Coogan et al., 2014; Roskosz et al., 2015; Sobolev et al., 2016). In the case of wehrlitic rocks (olivine $> 40\,\%$), the scarcity of orthopyroxene (less than $5\,\%$) with respect to the dominant clinopyroxene and the presence of spinel as an accessory mineral make the application of currently available oxythermobarometer (Eq. 1) very difficult.

In this study, we report for the first time in situ synchrotron Mössbauer measurements of (1) the Fe oxidation state of one olivine grain (three data points) and two spinel inclusions of 20–30 µm in size and (2) the Fe oxidation state of two spinels included in a second olivine host from the same wehrlitic sample. The obtained data were, then, integrated with an in situ micro-Fourier transform infrared spectroscopy (micro-FTIR) analysis on an inclusion-free olivine from the same rock sample, energy-dispersive spectroscopy (EDS) element mapping, and EPMA chemical analyses of 4 olivines and 12 spinel inclusions trapped in 2 of these olivines. Finally, we determined the f_{O_2} of the wehrlitic rock sample and discussed the results in terms of oxygen influx at the time of encapsulation of the investigated spinels.

2 Materials and methods

2.1 Mineral samples and provenance

The investigated samples consist of a wehrlitic xenolith from an ash-rich tuff phreatomagmatic deposit of the Lago Piccolo subsystem of the Vulture volcano district (Stoppa and Principe, 1997; Jones et al., 2000; Giannandrea et al., 2006; Carnevale et al., 2022). These ultramafic xenoliths are found as the core of the pelletal lapillus (Fig. 1a) brought to the surface from a depth of about 30 km during the last volcanic activity of Mt. Vulture (141 ± 11 ka; Villa and Buettner, 2009) even if the volcano is still degassing mantle-derived CO_2 (Caracausi et al., 2015). Four olivine single crystals (size ~ 300 µm) from these xenoliths were hand-picked to be representative of the whole wehrlitic sample. Three of the four selected olivine grains show a distribution of opaque spinels from euhedral to rounded in shape located near the rim (Fig. 1b). Once one of these was crushed (Olivine Vul_1), two spinel single crystals of 20–30 µm in size could be extracted (Ol1_Spinel_1 and Ol1_Spinel_2; Fig. 1c) using a needle, placed on an adhesive tape and mounted in a brass sample holder. Another two olivines with evidence of spinel inclusions (Olivine Vul_2 and Olivine Vul_3) were embedded in epoxy, along with an olivine free of inclusions (Olivine Vul_rock) and a fragment of Olivine Vul_1, and polished to expose the spinels. Two of the exposed spinels from the same olivine (Olivine Vul_2) were successively extracted (Spinel_5 and Spinel_6) with a needle and placed on adhesive tape like the previous inclusions.

2.2 Synchrotron Mössbauer measurements

In order to determine the $Fe^{3+} / \sum Fe$ ratio of the hand-picked spinel crystals (see Table 1) measurements were carried out by in situ synchrotron Mössbauer spectroscopy (SMS) at the ID18 Nuclear Resonance Beamline (Rüffer and Chumakov, 1996) of the European Synchrotron Radiation Facility (ESRF, Grenoble, France) during two different beam time sessions. The Mössbauer characteristic energy of 14.4 keV is obtained using the (111) Bragg reflection of a $^{57}FeBO_3$ single crystal mounted on a Wissel velocity transducer driven with a sinusoidal waveform at room temperature (Potapkin et al., 2012; Cerantola et al., 2015). The X-ray beam was focused using Kirkpatrick–Baez mirrors onto different areas of about 3×8 µm^2 during the first beam time session, and 6×15 µm^2 during the second beam time session, respectively, due to slight differences in the setup. The velocity scale was calibrated in the range -6 to 6 mm s^{-1} using a 25 µm thick α-Fe foil. Spectra were fitted using a full transmission integral with normalized Lorentzian-squared source lines through the MossA software package (Prescher et al., 2012). About an hour and half were required to collect each of the three spectra on one olivine grain (Olivine Vul_1) and the spectra from the spinel grains (Table 2). The collected SMS spectra were analyzed taking into account the weak absorption caused by the presence of tiny amount of Fe in the Be window installed along the X-ray path at the beamline (Mikhailenko et al., 2020).

2.3 Micro-transmittance Fourier transform infrared (FTIR) spectroscopy

The FTIR measurements on Olivine Vul_rock (inclusion-free; see Table 1) were performed at the SISSI beamline of the ELETTRA synchrotron (Trieste, Italy). This beamline is equipped with a FTIR spectrometer coupled to a collimated infrared radiation generated by the synchrotron light source. This setup generally provides a spatial resolution of 2 cm^{-1}, an exposed area down to 20 µm of diameter, and excellent signal / noise ratio, all conditions that cannot be achieved using a standard laboratory FTIR spectrometer allowing, therefore, the detection of OH^- bands along multiple transects in the investigated minerals. The data presented here were, however, collected using a Vertex 70V Bruker interferometer coupled with a conventional Globar infrared source, a Hyperion IR microscope and a mercury cadmium telluride (MCT) detector to focus and resolve the areas of interest in the full spectral range. A total of four spectra from Olivine Vul_rock were collected in transmission mode with a spectral resolution of 2 cm^{-1} and an exposed circular area of 40 µm. The signal was averaged three times for 128 scans (128 s) on each measurement spot. The spectra from the air were collected as a reference. The water concentration was determined according to the Lambert–Beer law based on Bell et al. (2003) calibration.

2.4 Electron probe micro-analyzer (EPMA) and energy-dispersive spectroscopy (EDS)

The chemical composition of olivines and spinels from the wehrlitic core of the pelletal lapillus was measured on polished olivine grains embedded in epoxy resin using the JEOL JXA-8200 electron microprobe available at the National Institute of Geophysics and Volcanology (INGV) of Rome (Fig. 2). The analytical conditions were 15 kV of accelerating voltage and 7 nA beam current with a focused beam spot of less than 2 µm. The employed standards were olivine for Si, Mg and Ni; chromite for Al, Fe, Cr, Mn; rutile for Ti; Na and K calibrated from a natural obsidian. The chemical composition of four olivines was analyzed, included the Olivine Vul_rock measured to verify the consistency with the olivines investigated by Carnevale et al. (2022; Table S1 of the Supplement). Four spinel inclusions (two for rim and core) from Olivine Vul_2 and five spinel inclusions (one for rim and core) from Olivine Vul_3 were analyzed. No composition of the two trapped spinels (Spinel_1 and Spinel_2 hosted in Olivine Vul_1; Table 2) is available, due to impossibility to recover the grains from the tape after the SMS analysis. Semi-quantitative point mea-

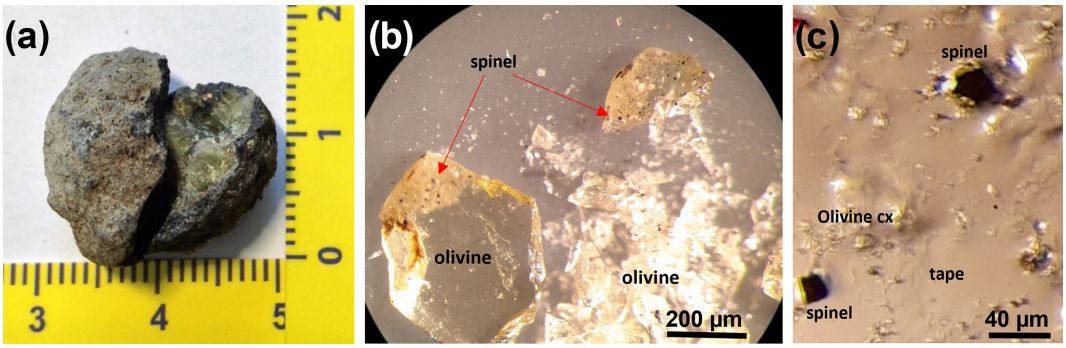

Figure 1. (a) Image of a lapillus with a wehrlitic core. **(b)** Olivine grains with tiny (< 40 µm) spinel inclusions (black dots). **(c)** Extracted spinels (Ol1_Spinel_1 and Ol1_Spinel_2) were placed on a Fe-free adhesive tape transparent to the X-rays.

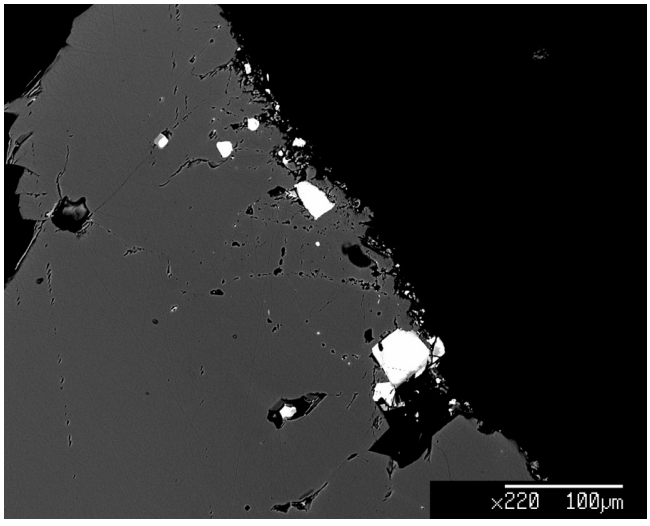

Figure 2. Back-scattered electron image of the analyzed Olivine Vul_2 (dark) and the spinel inclusions (bright) distributed along the olivine host rim with variable size.

surements and acquisition of chemical maps (Figs. S1–S3 of the Supplement) were also performed using the ZEISS EVO MA10 scanning electron microscope available at the Consiglio Nazionale delle Ricerche (CNR)–Istituto di Geologia Ambientale e Geoingegneria (IGAG; Rome) equipped with an AZTEC-integrated energy-dispersive X-ray spectrometer at 15 kV and 1.1 nA using cobalt as the standard for the EDS. The chemical maps were acquired to verify the presence of chemical zonation in two additional spinel inclusions from Olivine Vul_2 and in one spinel from Olivine Vul_3 (see notation in Table 1).

3 Results

3.1 Chemical composition of the investigated olivine host and spinel inclusions

The chemical composition of the investigated olivine grains and spinel inclusions are shown in Table 1 in terms of major oxides, Mg number (Fo) of olivine, and Cr and Mg number (i.e., Cr# and Mg#) of spinel. As can be seen from Figs. 1 and 2, the Cr-spinel inclusion appears semi-opaque to opaque, and it is embedded around the rim of the yellowish olivine phenocrysts. The Cr-spinel inclusions vary in shape from euhedral to rounded and are less than 100 µm in diameter (∼ 20–40 µm across but also smaller; Fig. 2). As previously mentioned, in order to compare the chemical composition of spinel inclusions in olivine, it is important to verify the chemical consistency of the selected olivine hosts with those reported by Carnevale et al. (2022) relative to the same wehrlitic olivines. Then, the spinels must also show clear evidence of their mantle origin.

Four analyzed olivine grains (see Table 1) collected from the same wehrlitic rock nodule reveal the same chemical composition with Mg# ranging from 89.7 to 90.7. The olivines have similar CaO contents compared to those from the olivine xenocrysts (Carnevale et al., 2022) but slightly higher contents than the core of the pelletal lapilli (Carnevale et al., 2022; Table S1) and those reported for wehrlitic olivines from samples aj24 and aj34 (Jones et al., 2000; Table S1). In Fig. 3a–d the Fo is plotted against CaO, NiO, MnO, and Al_2O_3. Figure 3a shows a correlation between Fo and CaO within the results of this study, which is otherwise absent in the case of NiO, MnO, and Al_2O_3 (Fig. 3b–d), where a general slight correlation is, in contrast, visible in literature data from Carnevale et al. (2022; C22) and Jones et al. (2000; J00) relative to the same Vulture wehrlitic nodules. Therefore, Fig. 3a–d provide evidence that, within the uncertainty of our measurements (Table 1), the analyzed olivines have compositions in good agreement with mantle olivines from the available data for Vulture xenoliths and show no chemical affinity with liquidus olivines having Mg# < 88

(Evans and Wright, 1972; Scowen et al., 1991; Kamenetsky et al., 2001).

Once the chemical homogeneity of the selected olivines is demonstrated, we proceed to discuss the composition of the spinel inclusions. The spinel inclusions in Olivine Vul_2 have a Cr# of 0.40–048 and a Mg# of 0.60–0.67 with no chemical variations observed in the two spinels where rim and core were measured, while a third spinel (Spinel_5 from Olivine Vul_2 in Table 1) shows a variation in both Cr# from 0.41 to 0.48 and Mg# from 0.60 to 0.67 (Fig. 4a) accompanied by an increase of Al_2O_3 from 27.30 wt % to 31.30 wt %. Spinels trapped in Olivine Vul_3 show more variability in terms of Cr# from 0.32 to 0.42, overlapping with the composition of spinel in Olivine Vul_2 with Mg# that varies from 0.62 to 0.66 within all the six analyzed spinels. We conclude that no significant variations are observed at the core and rim of two selected spinels (Spinel_1 and Spinel_6 from Olivine Vul_2 and Olivine Vul_3 of Table 1) confirming their mantle origin according to Arai (1994). The chemical maps shown in Figs. S1–S3 further exclude the presence of zoned spinels typical of liquidus chromites (Kamenetsky et al., 2001) granting, therefore, a mantle origin. Except for three spinels having Cr# < 0.38, the measured spinels have similar TiO_2 (0.41 wt %–0.60 wt %), MgO (16.00 wt %–19.40 wt %), and NiO (0.18 wt %–0.30 wt %) with respect to sample aj34 described by Jones et al. (2000), classified as a wehrlite, where minor amounts of orthopyroxenes and spinels are observed. Finally, a possible interaction with metasomatic mantle fluids can be inferred from Fig. 4a where the increase of Mg# with respect to Cr# (both from spinels) agrees with a Mg enrichment driven by metasomatic interaction (El Dien et al., 2019). Such interaction is confirmed also by the TiO_2 increase at almost constant FeO content in Fig. 4b according to Perinelli et al. (2008).

The homogeneity between the equilibrated olivine host and the spinel inclusions is shown through the diagrams $Mg\#_{spl}$ vs. Fo_{ol}, TiO_{2spl} vs. Al_2O_{3ol}, and $Cr\#_{spl}$ vs. Fo_{ol} (Fig. 5a–c). Such plots are usually presented to discriminate fast equilibration rather than crystallization from a melt inclusion (Wu et al., 2022). The narrow range of $Mg\#_{spl}$ within similar Fo_{ol} (Fig. 5a) supports the diffusive re-equilibration (e.g., Kamenetsky et al., 2001) owing to the rapid Fe–Mg interdiffusion rate between spinel and its host olivine at upper mantle temperatures (Ozawa, 1984). Such re-equilibration is not expected to vary much the Mg / Fe ratio of spinel, but it can cause a slight increase of Al in olivine (Wu et al., 2022). Generally, the selected spinel inclusions in olivine have lower TiO_2 and higher Al_2O_3 contents than those reported in spinel–olivine pairs of volcanic rocks used to retrieve the parental magma composition, but they match well with the values from peridotite rocks (Arai, 1994; Jones et al., 2000; Kamenetsky et al., 2001). The trends of decreasing Cr# versus Mg# in spinel (Fig. 4a) agree with what is generally reported in literature (see references in the legend of Fig. 4a) with spinel composition plotting along the olivine–spinel mantle array (OSMA), established by the relation between the Cr# and the Fo content of olivine host (Arai, 1994; El Dien et al., 2019). The Cr# of spinels from Olivine Vul_2 and Olivine Vul_3 overlaps, as well as the Fo of their olivine host (Fig. 5c). In conclusion, our data show the following:

1. The selected olivines have negligible chemical variation, so these are representative of the Vulture wehrlitic nodules.

2. The measured spinels are also homogeneous in composition and equilibrated at mantle conditions (likely recorded metasomatic interaction prior to entrapment in olivine; Fig. 4a–b).

3. There is consistency between the composition of the spinel inclusions investigated in this study and those reported for wehrlitic xenoliths by Stoppa and Principe (1997) and Jones et al. (2000) (Fig. 4a–b; see Table S2 in the Supplement).

This conclusion is enhanced by the absence of either significant core-to-rim chemical variation in spinels or the Mg# versus Fo positive correlation typical of liquidus minerals. According to Ballhaus et al. (1991) the (re-)equilibration T of the wehrlitic nodules is calculated to be 1060 °C.

3.2 Fe oxidation state in olivine host and spinel inclusions

The Mössbauer spectra were fitted with two doublets for Fe^{2+} and one for Fe^{3+} in the case of olivine (Figs. 6a and S4a–b of the Supplement) and with two doublets for Fe^{2+} and one for Fe^{3+} in the case of spinel (Figs. 6b and S4c–e of the Supplement). No magnetic contribution was observed in the spectra collected from the spinels. Table 2 summarizes the hyperfine parameters for each analyzed mineral and the calculated $Fe^{3+} / \sum Fe$. The quadrupole splitting (QS) and center shift (CS) are reported in Fig. 7a (olivine) and Fig. 7b (spinel) along with the hyperfine parameter from Canil and O'Neill (1996) and Ejima et al. (2018) for olivine and from Canil and O'Neill (1996) and Marras et al. (2023) for spinel, all related to literature spinels from mantle peridotites. The contribution of Fe from the Be window was taken into account when fitting the olivine and spinel spectra by including an extra singlet (CS of 0.2991 mm s^{-1}), based on background measurements performed during the analytical session. For the olivine, the $Fe^{3+} / \sum Fe$ ratio along a transect for a total of three points ranges between 0.03 and 0.05 ($\pm$ 0.01). The $Fe^{3+} / \sum Fe$ of the extracted spinel inclusions varies between 0.40 and 0.45 within an uncertainty of $\pm$ 0.02 except for spinel_6 from Olivine Vul_2, where the estimated error is $\pm$ 0.06 due to the lower signal-to-noise ratio of the acquired spectrum. By applying the correction proposed by De Grave and Van Alboom (1991) for the effect of temperature, namely for the different recoil-free fractions for Fe^{2+} and

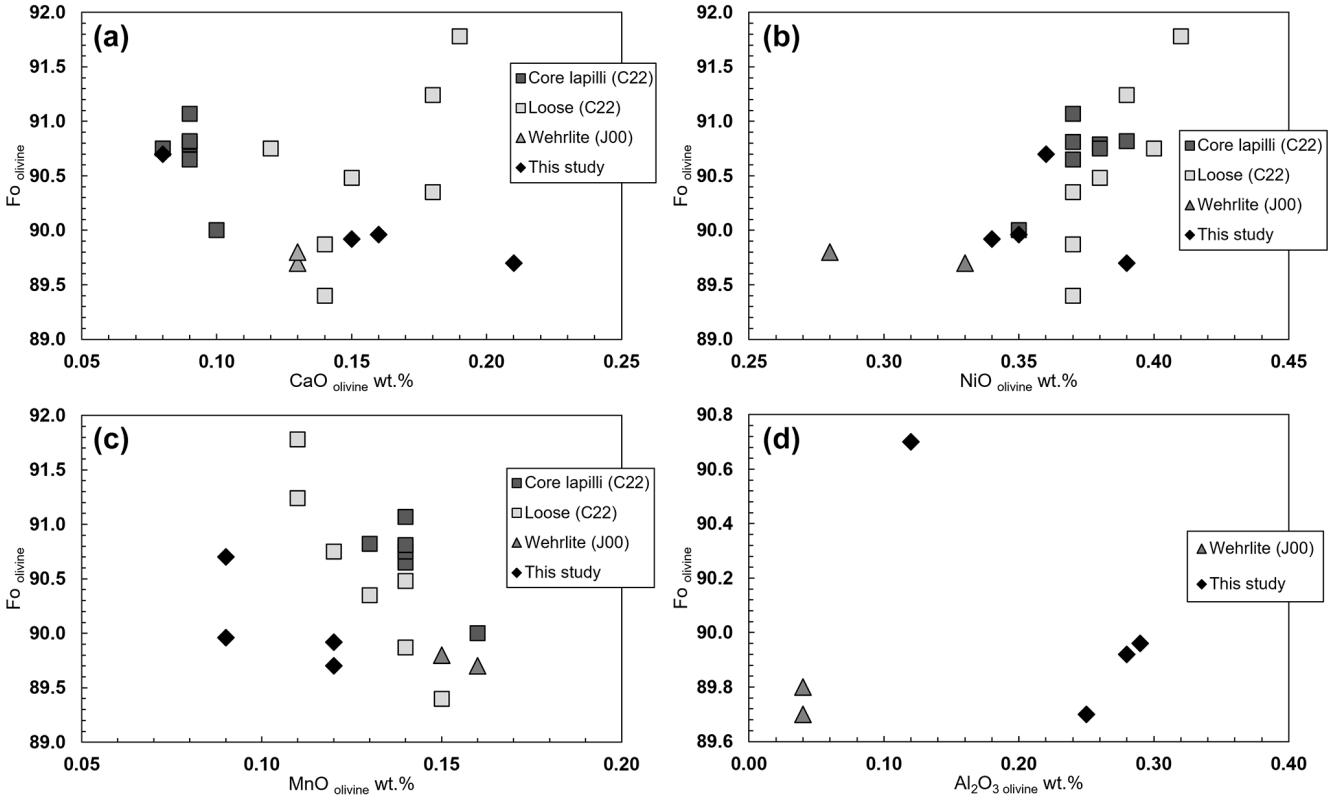

Figure 3. Fo olivine plotted against **(a)** CaO wt %, **(b)** NiO wt %, **(c)** MnO wt %, and **(d)** Al_2O_3 wt %, along with literature Vulture data from Jones et al. (2000; J00) and Carnevale et al. (2022; C22).

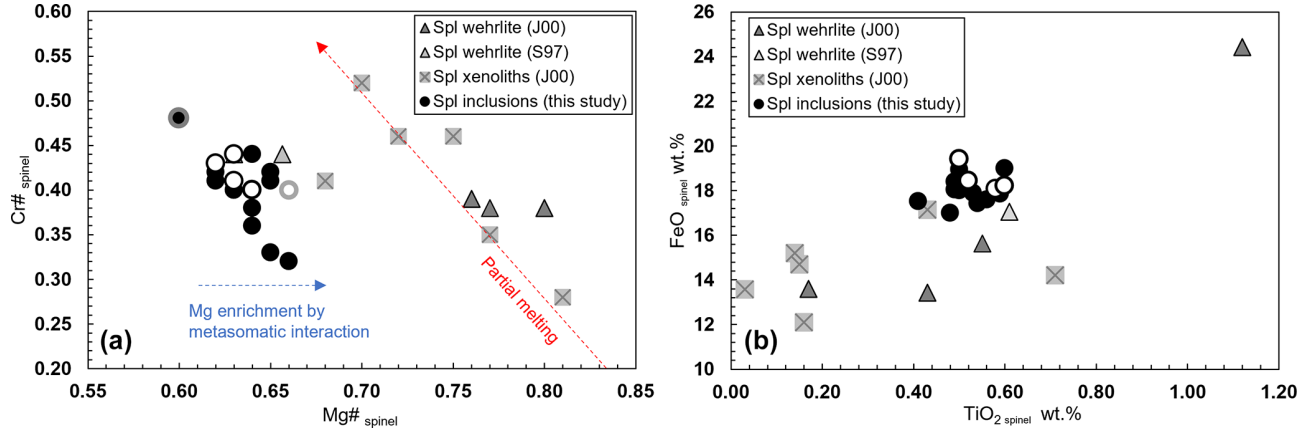

Figure 4. **(a)** Cr# vs. Mg# of spinel and **(b)** FeO wt % vs. TiO_2 wt % of spinel. Open symbols refer to rim measurements. Spinel 5 hosted in Olivine Vul_2 shows chemical variability among core and rim, and it is highlighted in grey. Literature data of Stoppa and Principe (1997; S97), Jones et al. (2000; J00), and Carnevale et al. (2022; C22) are also reported.

Fe^{3+}, our measured Fe^{3+} / $\sum$Fe ratios of spinel would decrease by about 0.05.

3.3 OH^- content of olivine

The water concentration of one inclusion-free olivine was estimated from the FTIR spectrum in Fig. 8 using the Lambert–Beer law according to Bell et al. (2003) calibration based on an integrated molar absorption coefficient of $28.450 \pm 1830\,L\,mol^{-1}\,cm^{-2}$ and thickness of the sample of $\sim 300\,\mu m$ in the case of unpolarized measurements. Interestingly, the collected spectrum shows a pattern very similar to the spectrum collected at 3.7 GPa on a slice cut parallel

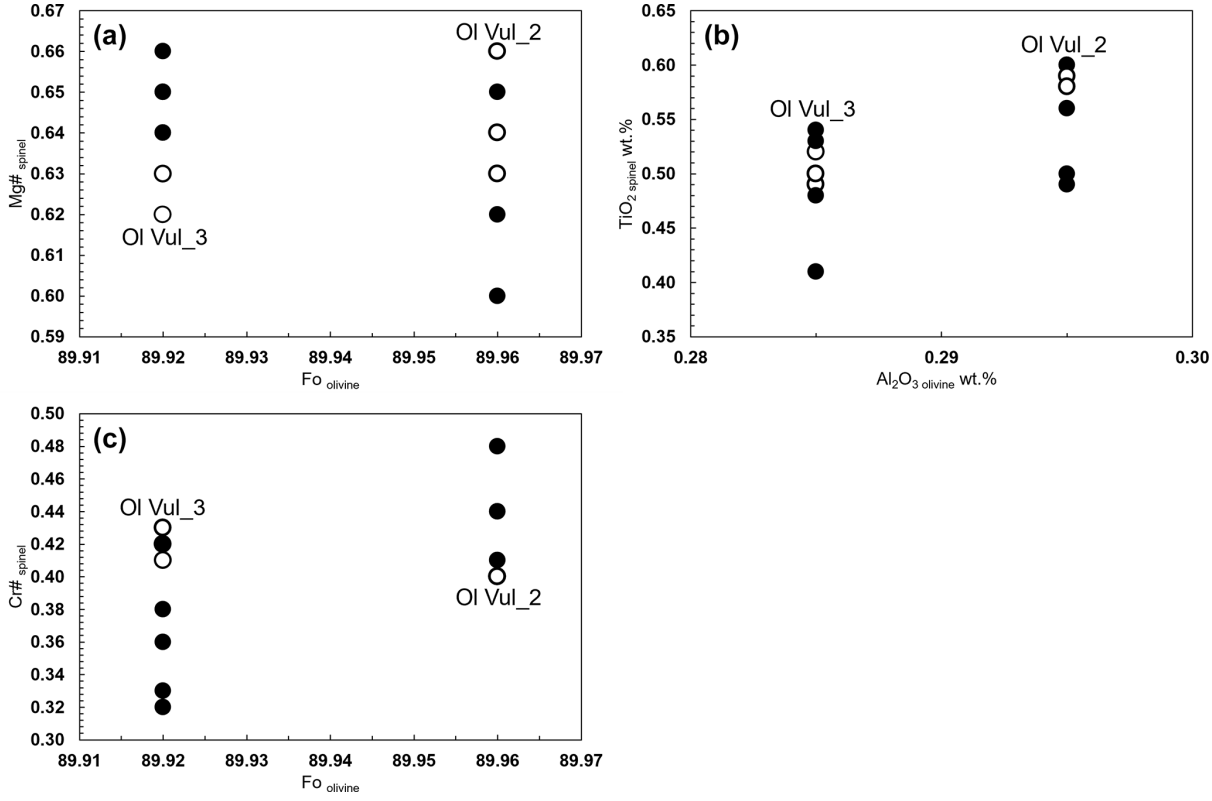

Figure 5. **(a)** Mg# spinel vs. Fo olivine, **(b)** TiO_2 wt % spinel vs. Al_2O_3 olivine, and **(c)** Cr# spinel vs. Fo for Olivine Vul_2 and Vul_3 and relative spinel inclusions. Open symbols refer to measurements at the rim of spinels.

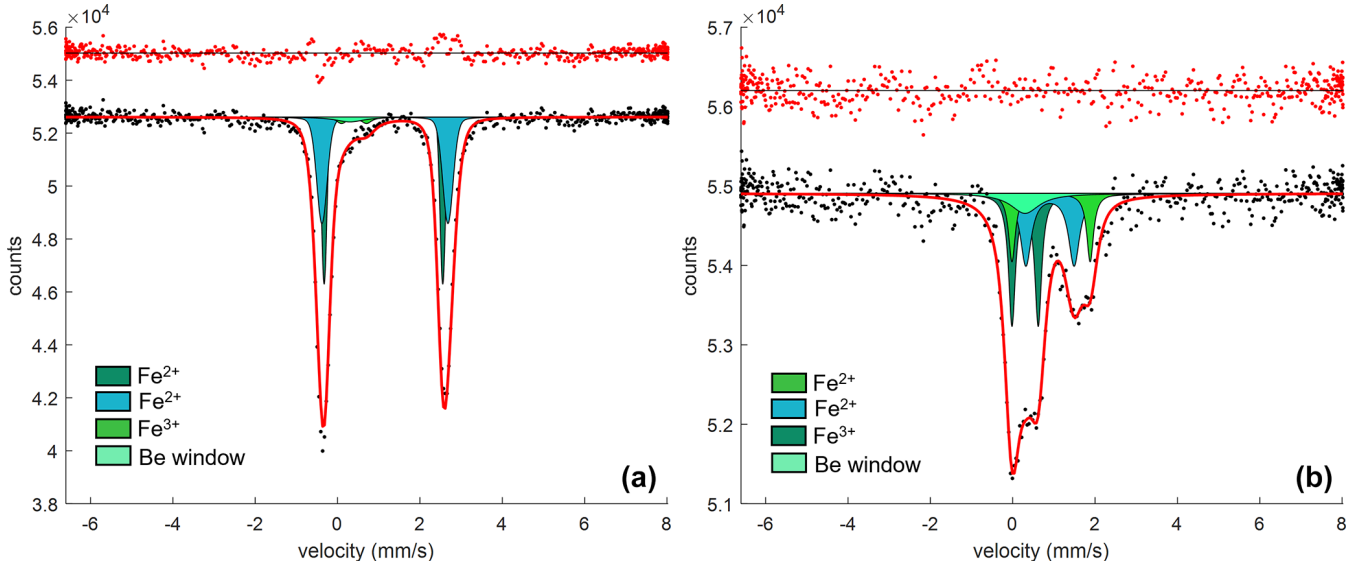

Figure 6. **(a)** SMS spectrum for Olivine Vul_1b (see Table 2) fitted with one doublet for Fe^{3+}, two doublets for Fe^{2+}, and one singlet for the Be window. **(b)** SMS spectrum for Spinel_1, fitted with one doublet for Fe^{3+}, two doublets for Fe^{2+}, and one singlet for Be window.

Table 1. Chemical composition (oxide wt %) of host olivines and spinel inclusions.

Sample	SiO_2	NiO	MgO	CaO	FeO	Al_2O_3	TiO_2	MnO	Cr_2O_3	Na_2O	K_2O	Total	Fo	
Olivine Vul_rock[a]	39.72	0.39	49.11	0.21	10.05	0.25	n.d.	0.12	0.13	0.03	0.00	100.01	89.70	
SD	0.67	0.01	0.30	0.03	0.09	0.03	0.00	0.07	0.02	0.01	0.01	0.69	0.17	
Host mineral														
Olivine Vul_1[b]	39.66	0.36	49.90	0.08	9.05	0.12	n.d.	0.09	0.02	n.d.	n.d.	99.30	90.7	
Olivine Vul_2[a]	40.08	0.35	49.49	0.16	9.84	0.29	0.01	0.09	0.11	0.06	0.03	100.48	89.96	
SD	0.20	0.10	0.24	0.03	0.69	0.06	0.02	0.04	0.10	0.01	0.00	0.61	0.65	
Olivine Vul_3[a]	40.10	0.34	49.21	0.15	9.83	0.28	0.03	0.12	0.11	0.03	0.05	100.23	89.92	
SD	0.12	0.07	0.26	0.06	0.19	0.07	0.05	0.03	0.03	0.01	0.04	0.43	0.20	
Sample	SiO_2	NiO	MgO	CaO	FeO	Al_2O_3	TiO_2	MnO	Cr_2O_3	Na_2O	K_2O	Total	Cr#	Mg#
Host: Olivine Vul_2														
Spinel 1	0.13	0.30	18.22	0.06	17.59	32.06	0.56	0.14	32.64	0.01	0.03	101.73	0.41	0.65
Spinel 2 core	0.07	0.30	17.43	0.03	17.86	31.22	0.59	0.22	32.87	n.d.	0.03	100.62	0.40	0.63
Spinel 2 rim	0.09	0.26	17.73	0.03	18.08	32.18	0.58	0.11	31.89	n.d.	0.04	100.98	0.40	0.64
Spinel 3	0.17	0.28	17.21	0.05	18.93	31.39	0.50	0.18	32.00	0.04	0.09	100.85	0.41	0.62
Spinel 4	0.14	0.18	17.43	n.d.	18.05	31.74	0.49	0.18	31.23	n.d.	0.02	99.46	0.40	0.63
Spinel 5 core[c]	–	–	16.00	–	18.90	27.30	–	–	37.80	–	–	100.00	0.48	0.60
Spinel 5 rim[c]	–	–	19.40	–	17.30	31.30	–	–	32.00	–	–	100.00	0.41	0.67
Spinel 6 core[c]	0.30	–	18.30	–	18.20	29.00	0.60	–	33.40	–	–	99.80	0.44	0.64
Spinel 6 rim[c]	1.00	–	18.30	–	19.00	27.90	0.60	0.30	32.80	–	–	99.90	0.44	0.63
Host: Olivine Vul_3														
Spinel 1 core	0.16	0.22	17.09	0.03	18.40	30.58	0.49	0.14	33.06	n.d.	n.d.	100.17	0.42	0.62
Spinel 1 rim	0.10	0.28	17.39	0.03	18.44	31.71	0.52	0.14	32.26	n.d.	n.d.	100.88	0.41	0.63
Spinel 2	0.23	0.23	18.24	0.04	16.99	38.15	0.48	0.17	26.30	0.02	0.01	100.87	0.32	0.66
Spinel 3	0.17	0.33	18.15	0.08	17.51	36.78	0.41	0.15	26.82	0.01	n.d.	100.41	0.33	0.65
Spinel 4	0.13	0.21	17.56	0.19	17.43	34.65	0.54	0.11	28.94	0.03	0.02	99.82	0.36	0.64
Spinel 5	0.21	0.35	17.92	0.02	17.89	33.08	0.53	0.15	30.51	0.02	0.01	100.68	0.38	0.64
Spinel 6 core[c]	0.30	–	18.50	–	18.00	30.20	0.50	–	32.40	–	–	99.90	0.42	0.65
Spinel 6 rim[c]	0.60	–	17.70	–	19.40	28.60	0.50	0.40	32.80	–	–	99.60	0.43	0.62

[a] Each analysis is the average of three data points. [b] Single measurement performed on an olivine fragment < 30 µm. [c] Spinels for which SEM analyses are shown here along with maps in the Supplement. n.d.: not detected. SD: standard deviation.

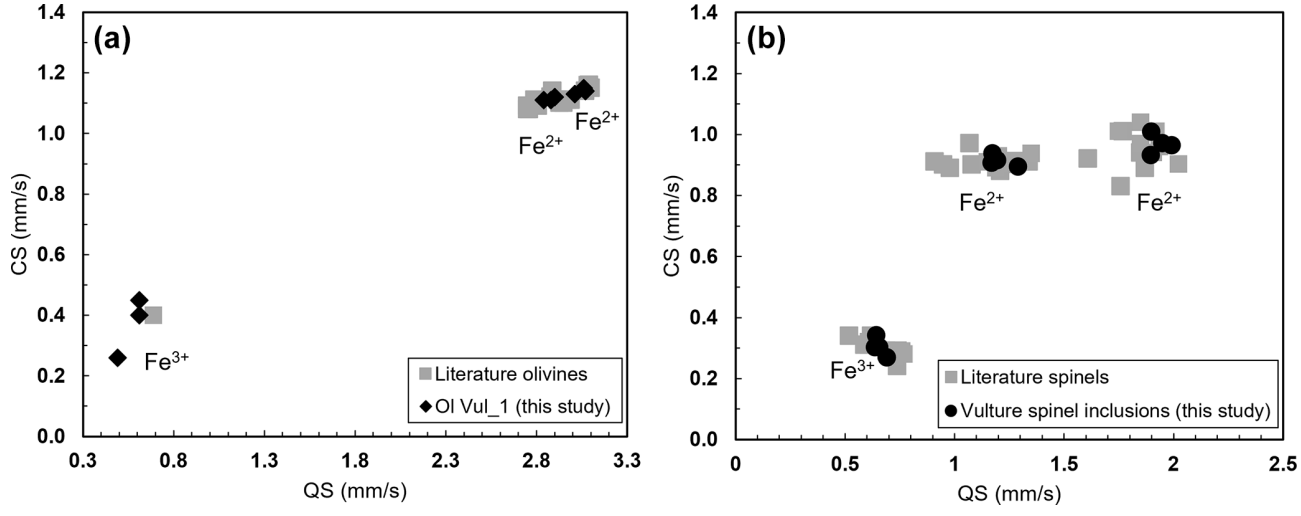

Figure 7. Hyperfine parameters (CS and QS) of the analyzed samples plotted with literature for **(a)** olivine (Canil and O'Neill, 1996; Ejima et al., 2018) and **(b)** spinel (Canil and O'Neill, 1996; Marras et al., 2023).

Table 2. Olivines (host) and spinels (inclusion) analyzed by in situ SMS along with the hyperfine parameters (central shift – CS, and quadrupole splitting – QS) and the relative Fe^{3+} / $\sum$Fe ratio.

Sample	Collecting time (h)	Assignment	CS ($mm\,s^{-1}$)	QS ($mm\,s^{-1}$)	Fe^{3+} / $\sum$Fe ratio
Olivine Vul_1a	1.5	Fe^{2+}	1.13	3.01	0.03 (1)
		Fe^{2+}	1.12	2.90	
		Fe^{3+}	0.26	0.49	
Olivine Vul_1b	1.5	Fe^{2+}	1.15	3.06	0.04 (1)
		Fe^{2+}	1.11	2.88	
		Fe^{3+}	0.40	0.61	
Olivine Vul_1c	1.5	Fe^{2+}	1.14	3.07	0.05 (1)
		Fe^{2+}	1.11	2.84	
		Fe^{3+}	0.45	0.61	
Host: Olivine Vul_1					
Ol1_Spinel_1[a]	1.5	Fe^{2+}	0.93	1.90	0.40 (2)
		Fe^{2+}	0.91	1.17	
		Fe^{3+}	0.30	0.64	
Ol1_Spinel_2[a]	1	Fe^{2+}	0.96	1.99	0.41 (2)
		Fe^{2+}	0.94	1.17	
		Fe^{3+}	0.34	0.64	
Host: Olivine Vul_2					
Spinel_5[b]	1.5	Fe^{2+}	0.97	1.95	0.45 (2)
		Fe^{2+}	0.89	1.29	
		Fe^{3+}	0.30	0.66	
Spinel_6[b]	1.5	Fe^{2+}	1.01	1.90	0.41 (6)
		Fe^{2+}	0.91	1.20	
		Fe^{3+}	0.27	0.69	

Estimated standard errors: CS $\pm$ 0.02 $mm\,s^{-1}$; QS $\pm$ 0.05 $mm\,s^{-1}$. [a] For these spinels no chemical data could be acquired. [b] The chemical composition and map are provided in Table 1 and the Supplement.

to (100) plane by Peslier et al. (2010). The calculated water content is 30 ppm, which is also well within the typical water content of olivines from peridotite xenoliths of ancient cratons (Peslier et al., 2010).

4 Discussion

4.1 Oxidation state of spinel inclusions and comparison with literature data

The Fe^{3+} / $\sum$Fe ratios measured in the olivine host and spinel inclusions are slightly higher but overall consistent with those reported by Ejima et al. (2018) and Canil and O'Neill (1996), respectively, in the case of mantle peridotites. The Fe^{3+} / $\sum$Fe of the included spinels is comparable to values reported by Jones et al. (2000; see their Table 6) on a stoichiometric basis ranging from 0.25 to 0.38. The Fe^{3+} / $\sum$Fe in spinel inclusions is also consistent with the general trend observed for spinel peridotites (Stagno, 2019). The $DFe^{3+}_{ol/spl}$ was not reported by Canil and O'Neill (1996) since no Fe^{3+} was detected in their olivines. Our Fe^{3+} / $\sum$Fe data from olivine (host) and spinel (inclusion) allow the determination of the $DFe^{3+}_{ol/spl}$, which ranges between 0.06 and 0.13, confirming that the amount of Fe^{3+} incorporated in mantle olivines is negligible. This $DFe^{3+}_{ol/spl}$ agrees with the 0.08 calculated from the Mössbauer data reported by Ejima et al. (2018) and collected on touching olivine and spinel from a lherzolite sampled in the Tariat Depression (Mongolia).

4.2 Oxythermobarometric implications and volatile speciation

The knowledge of the Fe^{3+} / $\sum$Fe in the spinel inclusions allows the calculation of the f_{O_2} of the mantle host rock according to Eq. (1). However, in order to apply Eq. (1), the presence and composition of the equilibrated orthopyroxene are required in order to assess the saturation of the sil-

ica activity (a_{SiO_2}) according to Ballhaus et al. (1991). The wehrlitic sample used in the context of this study does not contain visible orthopyroxene or spinel disperse in the matrix. However, we pointed out that our olivine and spinel inclusion compositions agree with those reported by Jones et al. (2000) for the same Vulture wehrlites where orthopyroxene is present and characterized by low compositional variations. Therefore, the absence of spinel occurring within the xenolith matrix is here overcome by the fact that the chemical composition of the investigated spinel inclusions is consistent with that of spinels from Vulture wehrlite, sample aj8, reported by Jones et al. (2000). The application of the spinel oxythermobarometer also requires the knowledge of the P–T conditions. In our case, we employ a P of 1.6–1.8 GPa and T of 1000–1100 °C as proposed by Jones et al. (2000) for wehrlite aj24 using different geothermobarometers (Wood and Banno, 1973 – TWB; Wells, 1977 – TW; Sachtleben and Secks, 1991 – TSS; Brey and Kohler, 1990 – TBXN; Köhler and Brey, 1990 – TCaOP; Mercier, 1980 – Men-sp; Mercier, 1980 – Mdi-sp). A preliminary determination of the $\log f_{O_2}$ results in values between 0.81 and 1.00 (± 0.6) log units above the FMQ reference buffer (O'Neill, 1987) using the calculated $Fe^{3+} / \sum Fe$ ratios in spinel inclusions (from of 0.40 and 0.45). The calculated $\log f_{O_2}$ of wehrlite aj7 for which Jones et al. (2000) provide the composition of olivine, orthopyroxene, and spinel is 0.85 log units (FMQ), consistent, therefore, with values obtained for our samples. The $Fe^{3+} / \sum Fe$ of spinel inclusions plotted versus the calculated $\log f_{O_2}$ agrees with the general trend observed for mantle peridotites (Stagno, 2019) (Fig. 9). It is noteworthy that these values are the highest compared to the f_{O_2} of spinel peridotites and plot above the water saturation curve determined along a typical geothermal gradient of 44 mW m^{-2} (Fig. 9; Stagno and Aulbach, 2021; Stagno and Fei, 2020). This is supported by the presence of H_2O in olivine, similar to that proposed by Peslier et al. (2010). Since this conclusion is based on H_2O measurement in one single olivine integrated with the determinations of $Fe^{3+} / \sum Fe$ in few spinel inclusions, obviously it would benefit from more statistically significant data. In this work, we provide a strong argument for a new way of obtaining f_{O_2} data from wehrlitic xenoliths using the $Fe^{3+} / \sum Fe$ determined in both olivine host and spinel inclusions in addition to their respective chemical compositions. The high Fe oxidation state in spinels included in olivine and their chemical composition along with the calculated $\log f_{O_2}$ support the geochemical evidence that these rocks would have experienced interaction with an oxidized metasomatic fluid (Bragagni et al., 2022). In particular, the CO_2-dominant nature of the fluid inclusions analyzed in olivines by Carnevale et al. (2022) coupled with the observation of carbonate-bearing microveins in Vulture olivines by Frezzotti and Touret (2014) highlights the possible presence of a carbonated fluid here supported by the high f_{O_2}.

To date, the f_{O_2} of wehrlitic rocks could not be calculated because of the lack of representative redox equilibria that can be either thermodynamically or experimentally calibrated. One possibility to overcome this issue is represented by the finding of rare orthopyroxene and spinel crystals equilibrated with the more abundant olivine and clinopyroxene. The opportunity to access to the composition of those spinels included in olivine showing a marked mantle affinity (i.e., entrapped by recrystallized olivines at mantle depths; Avè Lallement and Carter, 1970; Falus et al., 2011; Karato et al., 1980; Karato, 1988; Matthews et al., 2021) represents a valid tool to bypass such an issue. In the case of spinel inclusions in olivines from Vulture wehrlites, we propose that the f_{O_2} is that recorded at the time of the first interaction of the (spinel) peridotite with a carbonated oxidized fluid that, eventually, caused re-crystallization of olivine and entrapment of euhedral chromites. Alternatively, the spinel–olivine pairs might have recorded the oxidation event prior to the transport up to shallower conditions by a CO_2-bearing melt. If this was the case, either the olivine–spinel pair experienced very fast ascent by a low-viscosity magma in agreement with the fast ascent of the pristine magmas that transported to the surface the mantle materials (Carnevale et al., 2022) or they re-equilibrated at lithosphere–asthenosphere boundary (LAB) depths so as to retain their mantle affinity. In both cases, no chemical zonation is expected to form, which is what we show for the analyzed samples.

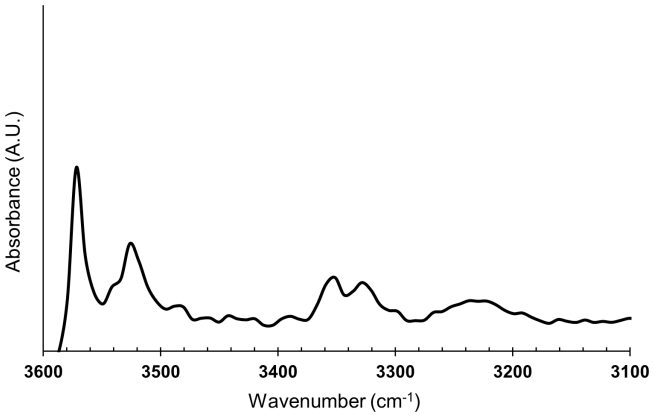

Figure 8. FTIR spectrum of olivine in the mid infrared region of fundamental O–H stretching vibrations.

5 Conclusions

We determined the Fe oxidation state of host olivine and spinel inclusions from Vulture wehrlite rock samples. The chemical analyses show evidence that these spinels are not liquidus chromites; rather they (re)equilibrated at mantle conditions, and likely they were entrapped during olivine recrystallization. The extracted spinels single crystals show high $Fe^{3+} / \sum Fe$ determined by in situ SMS that is higher than that reported in literature, resulting, therefore, in $\log f_{O_2} >$ FMQ buffer. We propose that these oxidized condi-

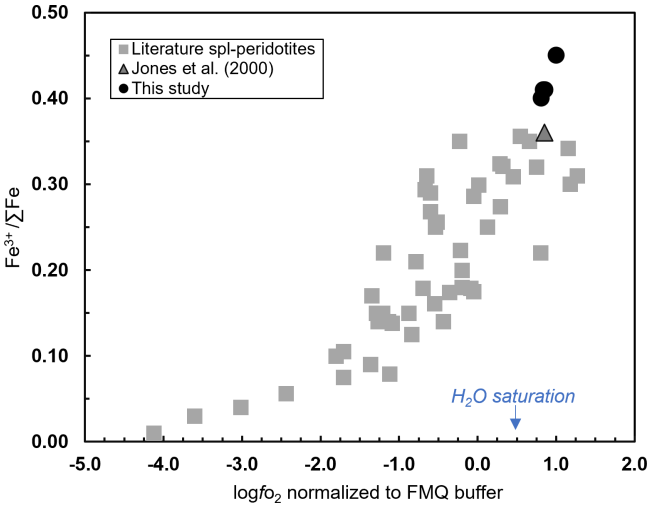

Figure 9. The spinel $Fe^{3+} / \sum Fe$ ratio against the $\log f_{O_2}$ for our Vulture wehrlite samples plotted along with literature data (Stagno, 2019, and references therein; Marras et al., 2023, and references therein). We estimated the $\log f_{O_2}$ for a wehrlite sample (aj7; Jones et al., 2000) according to the calculated spinel $Fe^{3+} / \sum Fe$ ratio at the proposed P and T conditions.

tions coupled with geochemical evidence of CO_2-dominant fluids trapped in olivine might originate from the interaction of the pristine lherzolite with a CO_2-rich metasomatic agent that occurred in the mantle either before the entrapment of spinel in olivine or prior to the transport of pair olivine–spinel to shallow depths. We point out the importance that the results from this study have in order to retrieve information about the redox state of mantle peridotites by measuring the $Fe^{3+} / \sum Fe$ and chemical composition of spinel inclusions in olivines.

Data availability. All data derived from this research are presented in the enclosed tables and figures and the Supplement.

Supplement. The supplement related to this article is available online at: https://doi.org/10.5194/ejm-35-665-2023-supplement.

Author contributions. GC, AC, and SR provided the samples and data employed for calculations. GM and VS performed chemical analysis by EMPA and collected and fitted the Mössbauer spectra. VS performed SEM semi-quantitative chemical maps. GM collected micro-FTIR spectra and elaborated the data. VS supervised the study and wrote the original draft together with GM. All the authors discussed the results, commented on the manuscript, and contributed to its final version.

Competing interests. The contact author has declared that none of the authors has any competing interests.

Disclaimer. Publisher's note: Copernicus Publications remains neutral with regard to jurisdictional claims in published maps and institutional affiliations.

Special issue statement. This article is part of the special issue "Probing the Earth: Melt and solid inclusions as probes to understand nature". It is not associated with a conference.

Acknowledgements. Giulia Marras and Vincenzo Stagno are grateful to Manuela Nazzari (INGV, Rome) for help during EPMA analyses and Matteo Paciucci (IGAG-CNR) for help with map acquisition. Part of this work was performed at beamline ID18 of ESRF (Grenoble, France) and SISSI (ELETTRA, Italy). The authors acknowledge the constructive comments of three anonymous reviewers and the editorial support provided by Matteo Alvaro and Elisabetta Rampone.

Financial support. This research has been supported by Fondi di Ateneo Sapienza 2021 to Vincenzo Stagno and the Ramón y Cajal research program (RYC2021-033270-I; MCIN/AEI/10.13039/501100011033 – EU NextGenerationEU/PRTR) to Antonio Caracausi.

Review statement. This paper was edited by Matteo Alvaro and reviewed by three anonymous referees.

References

Arai, S.: Characterization of spinel peridotites by olivine-spinel compositional relationships: review and interpretation, Chem. Geol., 113, 191–204, 1994.

Avé Lallemant, H. G. and Carter, N. L.: Syntectonic recrystallization of olivine and modes of flow in the upper mantle, Geol. Soc. Am. Bull., 81, 2203e2220, https://doi.org/10.1130/0016-7606(1970)81[2203:SROOAM]2.0.CO;2, 1970.

Ballhaus, C., Berry, R. F., and Green, D. H.: High pressure experimental calibration of the olivine-orthopyroxene-spinel oxygen geobarometer: implications for the oxidation state of the upper mantle, Contrib. Mineral. Petr., 107, 27–40, 1991.

Bell, D. R., Rossman, G. R., Maldener, J., Endisch, D., and Rauch, F.: Hydroxide in olivine: A quantitative determination of the absolute amount and calibration of the IR spectrum, J. Geophys. Res.-Sol. Ea., 108, 2105, https://doi.org/10.1029/2001JB000679, 2003.

Berry, A. J., O'Neill, H. S. C., Jayasuriya, K. D., Campbell, S. J., and Foran, G. J.: XANES calibrations for the oxidation state of iron in a silicate glass, Am. Mineral., 88, 967–977, 2003.

Bragagni, A., Mastroianni, F., Münker, C., Conticelli, S., and Avanzinelli, R.: A carbon-rich lithospheric mantle as a source

for the large CO_2 emissions of Etna volcano (Italy), Geology, 50, 486–490, 2022.

Brey, G. P. and Köhler, T.: Geothermobarometry in four-phase lherzolites, II. New thermobarometers, and practical assessment of existing thermobarometers, J. Petrol., 31, 1353–1378, 1990.

Canil, D. and O'Neill, H. S. C.: Distribution of ferric iron in some upper-mantle assemblages, J. Petrol., 37, 609–635, 1996.

Caracausi, A., Paternoster, M., and Nuccio, P. M.: Mantle CO_2 degassing at Mt. Vulture volcano (Italy): relationship between CO_2 outgassing of a volcano and the time since its last eruption, Earth Planet. Sc. Lett., 411, 268–280, 2015.

Carnevale, G., Caracausi, A., Rotolo, S. G., Paternoster, M., and Zanon, V.: New Inferences on Magma Dynamics in Melilitite-Carbonatite Volcanoes: The Case Study of Mt. Vulture (Southern Italy), Geophys. Res. Lett., 49, e2022GL099075, https://doi.org/10.1029/2022GL099075, 2022.

Cerantola, V., McCammon, C., Kupenko, I., Kantor, I., Marini, C., Wilke, M., and Dubrovinsky, L.: High-pressure spectroscopic study of siderite ($FeCO_3$) with a focus on spin crossover, Am. Mineral., 100, 2670–2681, 2015.

Coogan, L. A., Saunders, A. D., and Wilson, R. N.: Aluminum-in-olivine thermometry of primitive basalts: Evidence of an anomalously hot mantle source for large igneous provinces, Chem. Geol., 368, 1–10, 2014.

Cottrell, E., Kelley, K. A., Lanzirotti, A., and Fischer, R. A.: High-precision determination of iron oxidation state in silicate glasses using XANES, Chem. Geol., 268, 167–179, 2009.

Davis, F. A., Cottrell, E., Birner, S. K., Warren, J. M., and Lopez, O. G.: Revisiting the electron microprobe method of spinel-olivine-orthopyroxene oxybarometry applied to spinel peridotites, Am. Mineral., 102, 421–435, 2017.

De Grave, E. and Van Alboom, A.: Evaluation of ferrous and ferric Mössbauer fractions, Phys. Chem. Miner., 18, 337–342, 1991.

Droop, G. T. B.: A general equation for estimating Fe^{3+} concentrations in ferromagnesian silicates and oxides from microprobe analyses, using stoichiometric criteria, Miner. Mag., 51, 431–435, 1987.

Dyar, M., Gunter, M. E., Delaney, J. S., Lanzarotti, A., and Sutton, S. R.: Systematics in the structure and XANES spectra of pyroxenes, amphiboles, and micas as derived from oriented single crystals, Can. Mineral., 40, 1375–1393, 2002.

Dyar, M., Breves, E. A., Gunter, M. E., Lanzirotti, A., Tucker, J. M., Carey, J., Peel, E., Brown, E. B., Oberti, R., Lerotic, M., and Delaney, J. S.: Use of multivariate analysis for synchrotron micro-XANES analysis of iron valence state in amphiboles, Am. Mineral., 101, 1171–1189, 2016.

El Dien, H., Arai, S., Doucet, L. S., Li, Z. X., Kil, Y., Fougerouse, D., Reddy, S., Saxey, D. W., and Hamdy, M.: Cr-spinel records metasomatism not petrogenesis of mantle rocks, Nat. Commun., 10, 1–12, 2019.

Ejima, T., Osanai, Y., Akasaka, M., Adachi, T., Nakano, N., Kon, Y., Ohfuji, H., and Sereenen, J.: Oxidation states of Fe in constituent minerals of a spinel lherzolite xenolith from the Tariat Depression, Mongolia: the significance of Fe^{3+} in olivine, Minerals, 8, 204, https://doi.org/10.3390/min8050204, 2018.

Evans, B. W. and Wright, T. L.: Composition of liquidus chromite from the 1959 (Kilauea Iki) and 1965 (Makaopuhi) eruptions of Kilauea volcano, Hawaii, Am. Mineral., 57, 217–230, 1972.

Faccincani, L., Cerantola, V., Nestola, F., Nimis, P., Ziberna, L., Pasqualetto, L., Chumakov, A. I., Harris, J. W., and Coltorti, M.: Relatively oxidized conditions for diamond formation at Udachnaya (Siberia), Eur. J. Mineral., 34, 549–561, https://doi.org/10.5194/ejm-34-549-2022, 2022.

Falus, G., Tommasi, A., and Soustelle, V.: The effect of dynamic recrystallization on olivine crystal preferred orientations in mantle, J. Struct. Geol., 33, 1528–1540, 2011.

Fialin, M., Wagner, C., Métrich, N., Humler, E., Galoisy, L., and Bezos, A.: $Fe^{3+}/\Sigma Fe$ vs. Fe$L\alpha$ peak energy for minerals and glasses: Recent advances with the electron microprobe, Am. Mineral., 86, 456–465, 2001.

Frezzotti, M. L. and Touret, J. L.: CO_2, carbonate-rich melts, and brines in the mantle, Geosci. Front., 5, 697–710, 2014.

Frost, D. J.: The upper mantle and transition zone, Elements, 4, 171–176, 2008.

Giannandrea, P., La Volpe, L., Principe, C., and Schiattarella, M.: Unità stratigrafiche a limiti inconformi e storia evolutiva del vulcano medio-pleistocenico di Monte Vulture (Appennino meridionale, Italia), Boll. Soc. Geol. It., 125, 67–92, 2006.

Gudmundsson, G. and Wood, B. J.: Experimental tests of garnet peridotite oxygen barometry, Contrib. Mineral. Petr., 119, 56–67, 1995.

Hellebrand, E., Snow, J. E., Dick, H. J., and Hofmann, A. W.: Coupled major and trace elements as indicators of the extent of melting in mid-ocean-ridge peridotites, Nature, 410, 677–681, 2001.

Hoefer, H. E., Brey, G. P., and Woodland, A. B.: Iron oxidation state of mantle minerals determined from L emission spectra by the electron microprobe, International Kimberlite Conference: Extended Abstracts, Vol. 8, 2003.

Höfer, H. E. and Brey, G. P.: The iron oxidation state of garnet by electron microprobe: Its determination with the flank method combined with major-element analysis, Am. Mineral., 92, 873–885, 2007.

Jones, A. P., Kostoula, T., Stoppa, F., and Woolley, A. R.: Petrography and mineral chemistry of mantle xenoliths in a carbonate-rich melilititic tuff from Mt. Vulture volcano, southern Italy, Mineral. Mag., 64, 593–613, 2000.

Kamenetsky, V. S., Crawford, A. J., and Meffre, S.: Factors controlling chemistry of magmatic spinel: an empirical study of associated olivine, Cr-spinel and melt inclusions from primitive rocks, J. Petrol., 42, 655–671, 2001.

Karato, S. I.: The role of recrystallization in the preferred orientation of olivine, Phys. Earth Planet. Int., 51, 107e122, https://doi.org/10.1016/0031-9201(88)90029-5, 1988.

Karato, S. I., Toriumi, M., and Fujii, T.: Dynamic recrystallization of olivine single crystals during high-temperature creep, Geophys. Res. Lett., 7, 649e652, https://doi.org/10.1029/GL007i009p00649, 1980.

Kiseeva, E. S., Vasiukov, D. M., Wood, B. J., McCammon, C., Stachel, T., Bykov, M., Chumakov, A., Cerantola, V., Harris, J. W., and Dubrovinsky, L.: Oxidized iron in garnets from the mantle transition zone, Nat. Geosci., 11, 144–147, 2018.

Kiseeva, E. S., Korolev, N., Koemets, I., Zedgenizov, D. A., Unitt, R., McCammon, C., Aslandukova, A., Khandarkhaeva, S., Fedotenko, T., Glazyrin, K., Bessas, D., Aprilis, G., Chumakov, A., Kag, H., and Dubrovinsky, L.: Subduction-related oxidation of the sublithospheric mantle evidenced by ferropericlase and

magnesiowüstite diamond inclusions, Nat. Commun., 13, 7517, https://doi.org/10.1038/s41467-022-35110-x, 2022.

Köhler, T. P., and Brey, G.: Calcium exchange between olivine and clinopyroxene calibrated as a geothermobarometer for natural peridotites from 2 to 60 kb with applications, Geochim. Cosmochim. Ac., 54, 2375–2388, 1990.

Longo, M., McCammon, C. A., and Jacobsen, S. D.: Microanalysis of the iron oxidation state in (Mg, Fe)O and application to the study of microscale processes, Contrib. Mineral. Petrol., 162, 1249–1257, 2011.

Mallmann, G. and O'Neill, H. S.: Calibration of an empirical thermometer and oxybarometer based on the partitioning of Sc, Y and V between olivine and silicate melt, J. Petrol., 54, 933–949, 2013.

Marras, G., Stagno, V., Andreozzi, G. B., Caracausi, A., Cerantola, V., Frezzotti, M. L., Zacchigna, M., and Perinelli, C.: Extensive oxidizing events recorded by peridotite mantle xenoliths from the Hyblean Plateau: evidence from combined measurements of ferric iron in spinel with noble gases and fluid inclusions chemistry in olivine, Lithos, in review, 2023.

Matthews, S., Wong, K., Shorttle, O., Edmonds, M., and Maclennan, J.: Do olivine crystallization temperatures faithfully record mantle temperature variability?, Geochem. Geophy. Geosy., 22, e2020GC009157, https://doi.org/10.1029/2020GC009157, 2021.

McCammon, C. A.: A Mössbauer milliprobe: practical considerations, Hyperfine Interact., 92, 1235–1239, 1994.

McCammon, C. A., Beran, A., and Libowitzky, E.: Mössbauer spectroscopy: applications, Rev. Mineral. Geochem., 6, 369–398, 2004.

Mercier, J. C. C.: Single-pyroxene thermobarometry, Tectonophysics, 70, 1–37, 1980.

Mikhailenko, D. S., Stagno, V., Korsakov, A. V., Andreozzi, G. B., Marras, G., Cerantola, V., and Malygina, E. V.: Redox state determination of eclogite xenoliths from Udachnaya kimberlite pipe (Siberian craton), with some implications for the graphite/diamond formation, Contrib. Mineral. Petr., 175, 1–17, 2020.

Nestola, F., Cerantola, V., Milani, S., Anzolini, C., McCammon, C., Novella, D., Kupenko, I., Chumakov, A., Rüffer, R., and Harris, J. W.: Synchrotron Mössbauer Source technique for in situ measurement of iron-bearing inclusions in natural diamonds, Lithos, 265, 328–333, 2016.

O'Neill, H. S. C. and Wall, V.: The olivine–orthopyroxene–spinel oxygen geobarometer, the nickel precipitation curve, and the oxygen fugacity of the Earth's Upper Mantle, J. Petrol., 28, 1169–1191, 1987.

Ozawa, K.: Olivine-spinel geospeedometry: Analysis of diffusion-controlled Mg-Fe^{2+} exchange, Geochim. Cosmochim. Ac., 48, 2597–2611, 1984.

Perinelli, C., Sapienza, G. T., Armienti, P., and Morten, L.: Metasomatism of the upper mantle beneath the Hyblean Plateau (Sicily): evidence from pyroxenes and glass in peridotite xenoliths, Lond. Geol. Soc. Spec. Publ., 293, 197–221, 2008.

Peslier, A. H., Woodland, A. B., Bell, D. R., and Lazarov, M.: Olivine water contents in the continental lithosphere and the longevity of cratons, Nature, 467, 78–81, 2010.

Potapkin, V., Chumakov, A. I., Smirnov, G. V., Celse, J. P., Rüffer, R., McCammon, C., and Dubrovinsky, L.: The ^{57}Fe synchrotron Mössbauer source at the ESRF, J. Synchrotron. Radiat., 19, 559–569, 2012.

Prescher, C., McCammon, C., and Dubrovinsky, L.: MossA: a program for analyzing energy-domain Mössbauer spectra from conventional and synchrotron sources, J. Appl. Crystallogr., 45, 329–331, 2012.

Roskosz, M., Sio, C. K., Dauphas, N., Bi, W., Tissot, F. L., Hu, M. Y., Zhao, J., and Alp, E. E.: Spinel–olivine–pyroxene equilibrium iron isotopic fractionation and applications to natural peridotites, Geochim. Cosmochim. Ac., 169, 184–199, 2015.

Rudra, A., Cottrell, E., and Hirschmann, M. M.: Experimental determination of ferric iron partitioning between pyroxene and melt at 100 kPa, Chem. Geol., 584, 120532, https://doi.org/10.1016/j.chemgeo.2021.120532, 2021.

Rüffer, R., and Chumakov, A. I.: Nuclear resonance beamline at ESRF, Hyperfine Interact., 97, 589–604, 1996.

Sachtleben, T. and Seck, H. A.: Chemical control of Al-solubility in orthopyroxene and its implications on pyroxene geothermometry, Contrib. Mineral. Petr., 78, 157–165, 1981.

Schmid, R., Wilke, M., Oberhänsli, R., Janssens, K., Falkenberg, G., Franz, L., and Gaab, A.: Micro-XANES determination of ferric iron and its application in thermobarometry, Lithos, 70, 381–392, 2003.

Scowen, P. A. H., Roeder, P. L., and Helz, R. T.: Reequilibration of chromite within Kilauea Iki lava lake, Hawaii, Contrib. Mineral. Petr., 107, 8–20, 1991.

Sobolev, A. V., Asafov, E. V., Gurenko, A. A., Arndt, N. T., Batanova, V. G., Portnyagin, M. V., Garbe-Schönbergand, D., and Krasheninnikov, S. P.: Komatiites reveal a hydrous Archaean deep-mantle reservoir, Nature, 531, 628–632, https://doi.org/10.1038/nature17152, 2016.

Sobolev, V. N., McCammon, C. A., Taylor, L. A., Snyder, G. A., and Sobolev, N. V.: Precise Mössbauer milliprobe determination of ferric iron in rock-forming minerals and limitations of electron microprobe analysis, Am. Mineral., 84, 78–85, 1999.

Stagno, V.: Carbon, carbides, carbonates and carbonatitic melts in the Earth's interior, J. Geol. Soc. Lond., 176, 375–387, 2019.

Stagno, V. and Aulbach, S.: Redox Processes Before, During, and After Earth's Accretion Affecting the Deep Carbon Cycle, Magma Redox Geochem., 266, 19–32, 2021.

Stagno, V. and Fei, Y.: The redox boundaries of Earth's interior, Elements, 16, 166–172, 2020.

Stagno, V., Ojwang, D. O., McCammon, C. A., and Frost, D. J.: The oxidation state of the mantle and the extraction of carbon from Earth's interior, Nature, 493, 84–88, 2013.

Stoppa, F. and Principe, C.: Eruption style and petrology of a new carbonatitic suite from the Mt. Vulture southern Italy: The Monticchio Lakes Formation, J. Volcanol. Geotherm. Res., 78, 251–265, 1997.

Villa, I. M. and Buettner, A.: Chronostratigraphy of Monte Vulture volcano (southern Italy): Secondary mineral microtextures and ^{39}Ar–^{40}Ar systematics, Bull. Volcanol., 71, 1195–1208, 2009.

Wells, P. R.: Pyroxene thermometry in simple and complex systems, Contrib. Mineral. Petr., 62, 129–139, 1977.

Wilke, M., Farges, F., Petit, P. E., Brown Jr., G. E., and Martin, F.: Oxidation state and coordination of Fe in minerals: an Fe K XANES spectroscopic study, Am. Mineral., 86, 714–730, 2001.

Wilke, M., Partzsch, G. M., Bernhardt, R., and Lattard, D.: Determination of the iron oxidation state in basaltic glasses using XANES at the K-edge, Chem. Geol., 220, 143–161, 2005.

Wood, B. J. and Banno, S.: Garnet-orthopyroxene and orthopyroxene-clinopyroxene relationships in simple and complex systems, Contrib. Mineral. Petr., 42, 109–124, 1973.

Wood, B. J. and Virgo, D.: Upper mantle oxidation state: Ferric iron contents of lherzolite spinels by ^{57}Fe Mössbauer spectroscopy and resultant oxygen fugacities, Geochim. Cosmochim. Ac., 53, 1277–1291, 1989.

Wu, Y. D., Yang, J. H., Stagno, V., Nekrylov, N., Wang, J. T., and Wang, H.: Redox heterogeneity of picritic lavas with respect to their mantle sources in the Emeishan large igneous province, Geochim. Cosmochim. Ac., 320, 161–178, 2022.